Measurement of the Average Two-Dimensional Surface Temperature Distribution of Drops in a Melt Atomization Process

Clemens Kirmse and Humberto Chaves

(Submitted July 29, 2014; in revised form December 4, 2014)

During the production of metal and alloy powders by melt atomization, the knowledge of the surface temperature distribution of drops is essential. This paper shows the application of low-cost industrial CCD-cameras in connection with advanced image processing techniques to measure the average two-dimensional surface temperature distribution of drops in a melt atomization process. These measurements are necessary for comparison with the results of numerical investigations. The two-color pyrometer consists of two standard industrial CCD-cameras with appropriate optical filters. After calibration using a high-temperature furnace, the relative measurement error was smaller than 1.6% within the temperature range of 1273-1873 K. The pyrometer was applied to measure the average temperature distribution during the metal spraying process in a vacuum inert gas atomization facility. The measured temperature distribution averaged over 10 ms shows the development of a hollow cone spray of the atomized metal. The average axial distance between the atomization nozzle and the region of the liquidus temperature was found to be approximately 40 times the diameter of the atomization nozzle.

1. Introduction

Metal and alloy powders are predominantly produced by melt atomization (Ref 1). The goal of this process is the manufacturing of particles with preferably small diameters where the temperature distribution within the metal spray is of great influence. To control the atomizing spray process, the measurement of the particle temperature is essential. Thereby, it is important to distinguish between single particle and ensemble methods (Ref 2, 3). The temperature measurement of single particles requires ambitious high-speed equipment since the particle velocity near the atomization nozzle is in the region of some hundreds meter per second. In contrast, temperature measurement by ensemble methods is possible at lower costs. Especially the availability of low-cost digital cameras in connection with advanced image processing techniques permits the development of inexpensive measurement devices.

This paper describes the design and application of an optical two-color pyrometer for two-dimensional averaged temperature measurements of drops in melt atomization.

Clemens Kirmse and **Humberto Chaves**, Institute of Mechanics and Fluid Dynamics, Technical University Bergakademie of Freiberg, Freiberg, Germany. Contact e-mail: Clemens.Kirmse@imfd.tu-freiberg.de.

Nomenclature

$E_{b,\lambda}$ (W/m^3)	Spectral blackbody emissive power
$C_1 = 2\,h\,c_0^2$ (W/m^2)	Constant #1 with Planck's constant h and the velocity of light under vacuum conditions c_0
$C_2 = h\,c_0/K_B$ (K m)	Constant #2 with Boltzmann constant K_B
λ (m)	Wavelength
T (K)	Temperature
ε (-)	Emissivity
I_λ	Gray-level intensity of the measured signal
$R = I_{\lambda 1}/I_{\lambda 2}$ (-)	Intensity ratio
K (-)	Specific instrumentation constant
$S_R = K_1/K_2$ (-)	Correction term
T_{calib} (K)	Temperature of the measurement after calibration
T_{furn} (K)	Temperature of the furnace
T_{liq} (K)	Liquidus temperature of a melt
t_{imag} (s)	Image acquisition time
Δz (m)	Total depth of field
p (m)	Pixel size of the camera sensor
$f\#$ (-)	f-number of the objective
β (-)	Lateral magnification
d (m)	Diameter of the atomization nozzle

It consists of two standard industrial CCD-cameras with appropriate optical filters. After calibration using a high-temperature furnace, the pyrometer was applied to measure the average temperature distribution during the me-

tal spraying process in a vacuum inert gas atomization facility.

2. Experimental Set-Up

2.1 Basics of Two-Color Pyrometry

Temperature measurement by means of pyrometry is based on the measurement of electromagnetic radiation. Each body with a temperature $T > 0$ K emits electromagnetic radiation. The spectral emissive power rises with increasing temperature and the peak wavelength decreases. Planck's distribution law describes the spectral emissive power $E_{b,\lambda}$ of a blackbody:

$$E_{b,\lambda} = C_1 / (\lambda^5 (\exp(C_2/(\lambda T))) - 1) \qquad \text{(Eq 1)}$$

Wien's approximation simplifies Planck's equation:

$$E_{b,\lambda} = C_1 / (\lambda^5 \exp(C_2/(\lambda T))) \qquad \text{(Eq 2)}$$

This simplification is valid for $C_2/(\lambda T) \gg 1$, which is ensured for temperatures below 1900 K.

Up to now these equations refer to the maximum possible radiation of a blackbody. Real materials emit radiation with lower intensity. The ratio of the emitted radiation intensities between a real body and a blackbody is defined as the emissivity ε.

In the general case, the emissivity of a real surface is a function of the temperature, the wavelength, the material and its surface property, and the solid angle of its radiation.

The basics of two-color pyrometry consist in the simultaneous measurement of the spectral energy (intensity) at two different wavelengths (Ref 4, 5):

$$I_{\lambda 1} = K_1 \varepsilon_1 C_1 / (\lambda_1^5 \exp(C_2/(\lambda_1 T))) \qquad \text{(Eq 3)}$$

$$I_{\lambda 2} = K_2 \varepsilon_2 C_1 / (\lambda_2^5 \exp(C_2/(\lambda_2 T))) \qquad \text{(Eq 4)}$$

It is common to assume that ε_1 is approximately equal to ε_2 provided that the difference between the two wavelengths is sufficiently small. Then it is possible to calculate a temperature T_{calib} of the measurement after calibration and determining of the correction term S_R using the intensity ratio R:

$$R = I_{\lambda 1}/I_{\lambda 2} = S_R (\lambda_2/\lambda_1)^5 \exp(C_2(1/\lambda_2 - 1/\lambda_1)/T) \qquad \text{(Eq 5)}$$

$$T_{\text{calib}} = C_2(\lambda_1 - \lambda_2) / (\lambda_1 \lambda_2 (\ln(R) - \ln(S_R) + 5 \ln(\lambda_1/\lambda_2))) \qquad \text{(Eq 6)}$$

2.2 Setting of the Two-Color Pyrometer

The two-color pyrometer is built up of two industrial digital cameras, two optical filters, a beam splitter, and a combination of two lenses as object lens. The prerequisite for using these components is their sufficient optical transmission in the range of the selected filter wavelengths. During the metal spraying experiments, the liquid steel alloy is superheated to approximately 200 K above liquidus temperature and reaches a maximum value of 1873 K. Then the maximum of the spectral emissive power is close to the wavelength of 1.5 μm. The spectral sensitivity range of a usual image sensor is between 0.4 and 1.0 μm. Therefore, only a fraction of the emitted radiation intensity is recorded by the camera and yields smaller values of the pixel intensity. This has to be compensated by an enlarged exposure time.

The selected cameras are "mvBlueFox-224G" high-resolution gray scale CCD-cameras with 1600×1200 pixels (MATRIX VISION GmbH, Germany). The square unit cell size is 4.4 μm and the maximum frame rate is 16 fps. The images are saved as gray pictures with a resolution of 8 bit. The spectral sensitivity characteristics of the progressive scan CCD image sensor (SONY, ICX274AL) show the maximum relative response (100%) at a wavelength of 500 nm and an approximately linear decrease down to 950 nm and 5% relative response. The image acquisition is controlled by external triggering using a TTL signal generator. The start of acquisition is fired manually but every other TTL signal from a suitable source can be used.

The optical filters are dielectric bandpass filters (Thorlabs Inc., Newton, NJ, USA). They have center transmission wavelengths at $\lambda_1 = (850 \pm 8)$ nm and $\lambda_2 = (900 \pm 8)$ nm. The respective bandwidth (full width at half maximum) is (40 ± 8) nm. These wavelengths are located within the spectral sensitivity range of the image sensor of the cameras. The difference of the wavelengths is 50 nm. Therefore, the assumption of an approximately constant value of the emissivity at these wavelengths is possible.

The complete set-up of the two-color pyrometer is shown in Fig. 1. The image of the object is focused by an objective "Rollei-HFT Distagon 2.8/35". A biconcave lens is necessary to shift the focused images far enough from the lenses to allow the mounting of a beam splitter cube between the objective and the camera sensor chips. The beam splitter splits the optical path and the two images reach the camera sensors after passing the optical filters.

2.3 Image Pre-processing

The image acquisition of the two cameras is controlled by means of an external TTL signal generator. The trigger makes sure that the images are taken simultaneously. Because of the acquisition of the two images occurs on two different sensors the pixel-wise congruence of the images has to be established. This spatial calibration uses a calibration object which is usually a plane checkerboard. The images of the checkerboard are compared using a special algorithm in computer vision. The method of scale-invariant feature transform (SIFT) detects local features (e.g., corners of the chessboard) in the images (Ref 6). The result is the calculation of the homography matrix (perspective map) which includes the differences in translation and rotation between the two images (Ref 7). Using this matrix the images of one camera are transformed to match the images of the other camera. After this procedure, the images of the two cameras coincide with a pixel deviation smaller than one.
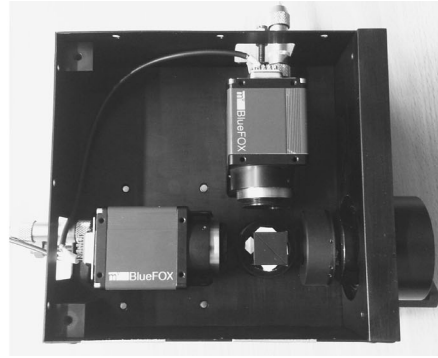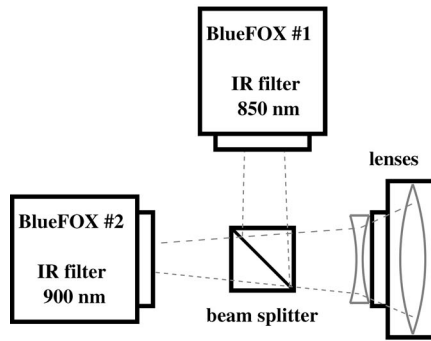
Fig. 1 Sketch (left) and picture (right) of the two-color pyrometer
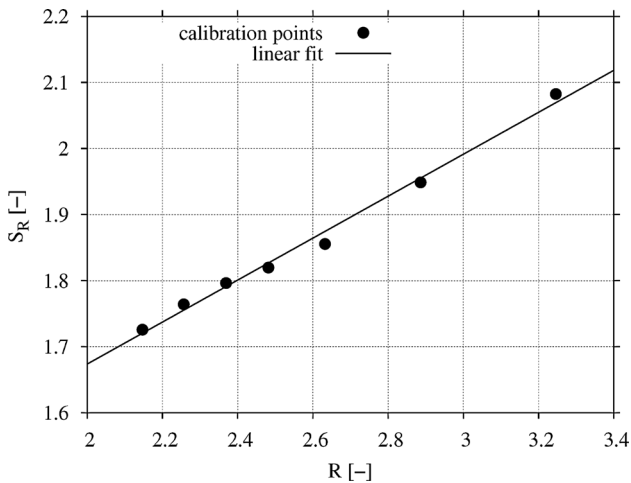
Fig. 2 Correction term S_R as a function of the intensity ratio R with the calibration points and the evaluated linear fitted line
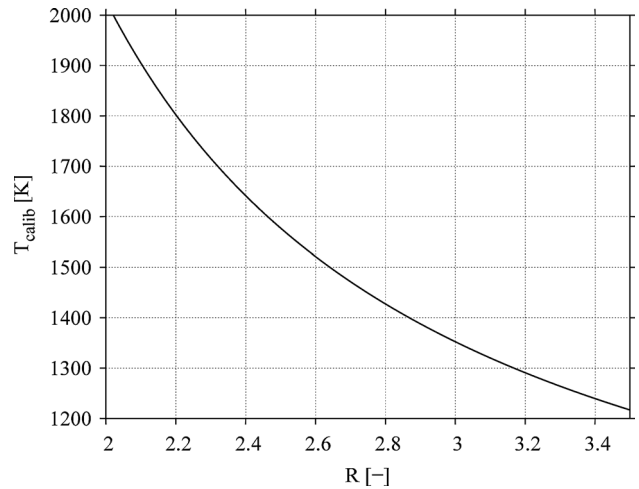
Fig. 3 Range of the calibrated temperature T_{calib} as a function of the intensity ratio R

2.4 Calibration and Error Estimation

The thermal calibration of the two-color pyrometer was performed using a high-temperature furnace. A hollow probe of silicon carbide was placed inside of the furnace chamber. The pyrometer was focused through a little hole of the probe on its inner surface. Thus, the thermal radiation was approximately like the radiation of a blackbody. T_{furn} was measured with a type B thermocouple (Pt30Rh-Pt6Rh) inside of the hollow probe. The absolute error of the temperature measurement was ±1.5 K. The calibration was performed in the temperature range from $T_{furn} = 1273$-1873 K with an increment of 100 K. For each measured temperature T_{furn}, the corresponding correction term $S_R(T_{furn})$ was calculated as follows:

$$S_R(T_{furn}) = R(T_{furn})\,(\lambda_1/\lambda_2)^5/\exp(C_2(1/\lambda_2 - 1/\lambda_1)/\,T_{furn}) \quad \text{(Eq 7)}$$

In Fig. 2, the relation between the correction term S_R and the intensity ratio R is shown for the case with an exposure time of 10 ms. It is obvious that a linear fit is sufficient for an arithmetic expression of the overall function

$$S_R = 1.039 + 0.317R \quad \text{(Eq 8)}$$

within the calibrated temperature range. Applying this relation to the measured intensity ratios results in corrected temperatures after calibration T_{calib}. The dependency between T_{calib} and the intensity ratio R for this case is shown in Fig. 3. A comparison between T_{furn} (measured by thermocouple) and T_{calib} (calculated by Eq 6 after inserting of Eq 8) is depicted in Fig. 4. Then the relative measurement error of T_{calib} can be calculated as follows:

Percent of measurement error of T_{calib}
$$= 100\% \,|\, T_{furn} - T_{calib}|/T_{furn} \quad \text{(Eq 9)}$$

In Fig. 5, this relative measurement error with a maximum of 1.6% is shown.

The limitation to the temperature range from 1273 to 1873 K is due to the furnace used to calibrate the system. This range is sufficient for measurements in spraying of molten steel as described in the following section of this paper. Another possibility to calibrate the two-color pyrometer is the application of a tungsten ribbon lamp which extends the calibrated temperature range to approximately 2800 K, (Ref
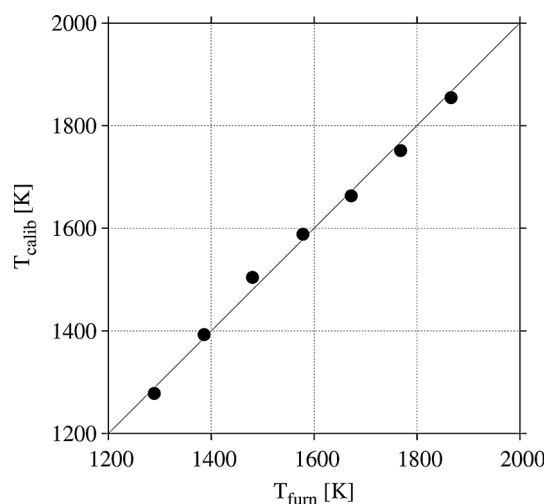
Fig. 4 Comparison between the calculated temperature of the two-color pyrometer T_{calib} and the temperature within the furnace T_{furn} quantified by a type B thermocouple
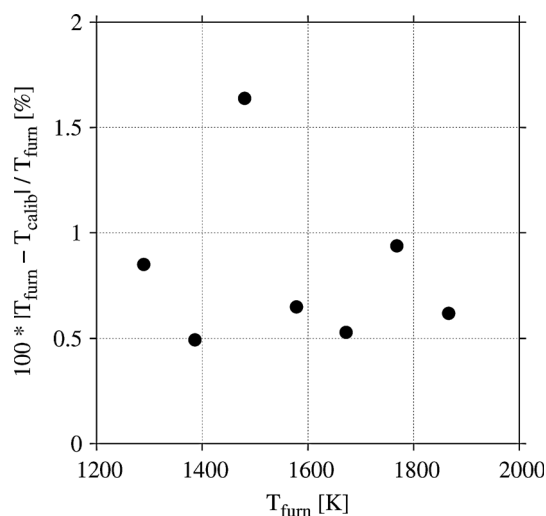

Fig. 5 Relative error of the measured temperature of the two-color pyrometer T_{calib} compared with the furnace temperature T_{furn}

8). The pyrometer can be used for measurements in other applications like high-velocity oxy-fuel (HVOF) sprays. Combined with measurements of the two-dimensional particle velocity distribution using particle image velocimetry (Ref 9) at the same time, two of the most important parameters of this spray process can be determined.

3. Results

The two-color pyrometer was applied to investigate the temperature distribution of a molten metal spray. Metal
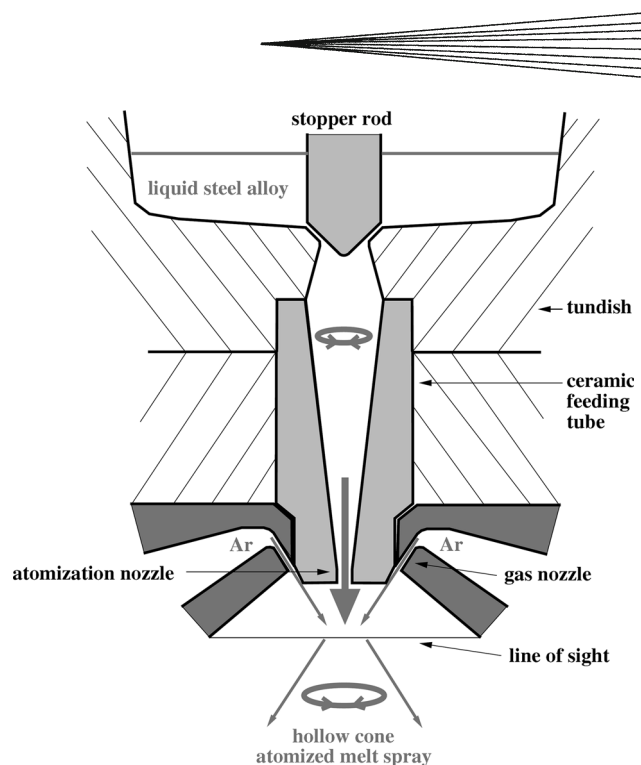
Fig. 6 Sketch of the vacuum inert gas atomization facility

spraying was performed by means of a vacuum inert gas atomization facility (ALD Vacuum Technologies GmbH, Hanau, Germany), Fig. 6. This typical process of metal spraying is given by the manufacturer. Therefore, only small variation of the spray parameter can be expected. In the following, the results of an example measurement are described. The liquid steel alloy was superheated to approximately 200 K above liquidus temperature in the tundish, (Ref 10). Thus, the maximum temperature of the melt was 1873 K. After reaching this temperature, the stopper rod was lifted and the liquid metal flowed under gravity through a conical ceramic feeding tube. At its bottom, a circular array of stainless steel nozzles is arranged. Argon gas streamed with constant high pressure of 2.6 MPa through the gas inlet into the nozzle. The interaction between the pre-filmed metal flow and the gas jets caused disintegration into metal droplets and ligaments. This configuration is typically for a close-coupled (confined) gas atomizer, (Ref 1, 11, 12).

In Fig. 7, the result of the temperature measurement using the two-color pyrometer is shown. The metal alloy was CrMnNi steel (16/7/6) with a liquidus temperature of 1673 K. The images were recorded with a frame rate of 10 fps and an exposure time of 10 ms per frame. The relatively long exposure time conforms to the conditions for calibration. Thus, the maximum intensity gray level of the images remains below the maximum value of 255 and an over-exposure is avoided. Otherwise, the exposure time is too long for recording the single metal drops moving with high velocities. Therefore, the recorded images show time-averaged gray-level values which also result in time-averaged temperature distributions of the droplet surface temperature.
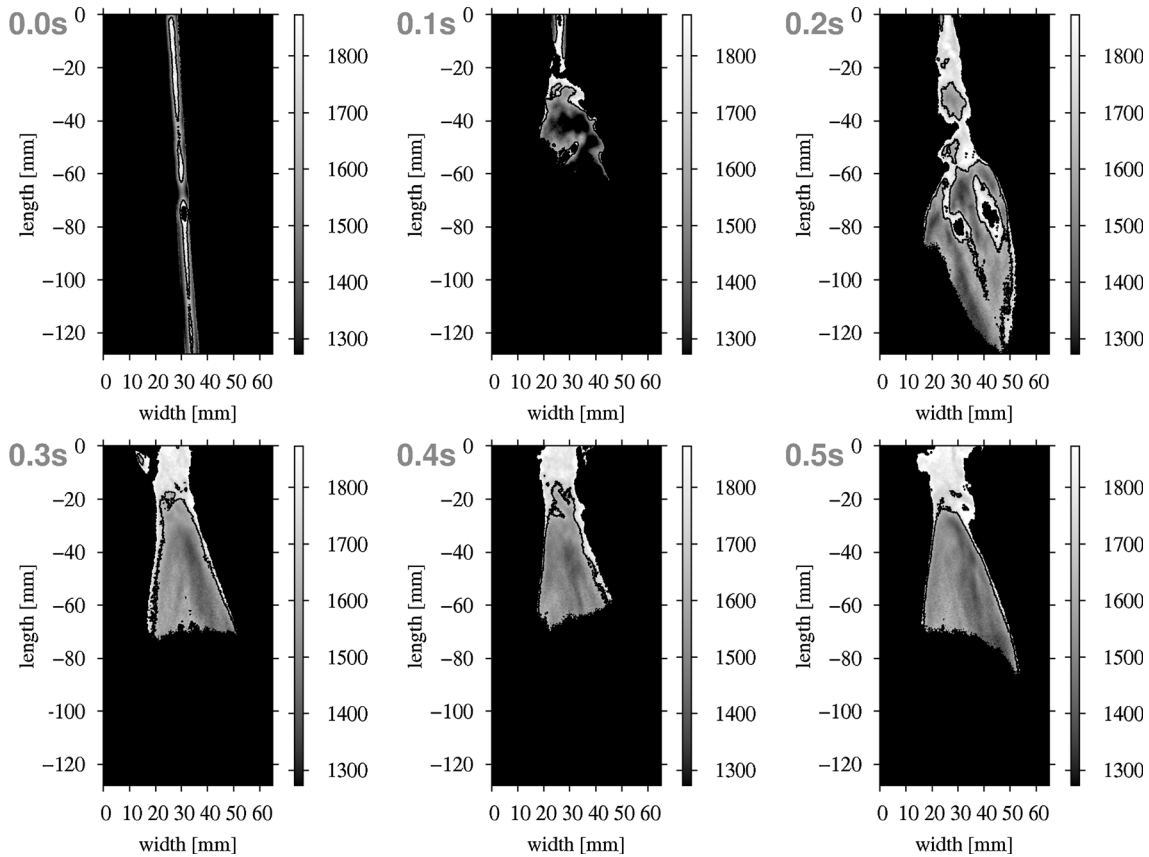
Fig. 7 Contour maps of the two-dimensional temperature measurement (in K) of the melt atomization. The quantity in the upper left corner of each temperature distribution is the image acquisition time t_{imag}. The black line within the region of the spray denotes the iso-line of the liquidus temperature of 1673 K. The black background means all temperatures are smaller than 1273 K which are out of the measurement range of the pyrometer

The field of view of the entire image was 0.12 m × 0.16 m with a distance of 0.73 m between the camera lens and the metal nozzle. The depth of field (DOF) of the pyrometer is mainly determined by the lens (objective) aperture diameter. Because of the relatively small radiation intensity in the region of λ_1 and λ_2 there are only two possibilities for a sufficient modulation of the images: (a) an increase in the exposure time or (b) an enlargement of the aperture diameter using the f-stop. In case (a), it would result in a longer time-averaging of the temperature distributions. In case (b), a lower f-number is due to a larger aperture diameter but yields a smaller DOF.

These measurements were performed using the pyrometer which operated in case (b). An estimation of the actual DOF can be arranged by applying a relation specified in (Ref 13, p. 77):

$$\Delta z = 2 p f \# (1 - \beta) / \beta^2 \qquad (\text{Eq 10})$$

With the pixel size of $p = 4.4$ μm as required sharpness, the f-number of the fully opened objective $f\# = 2.8$ and the lateral magnification $\beta = -0.044$ (1 mm in the object plane is equivalent to 10 pixel separation in the image plane) the total DOF Δz is then equal to 13 mm. Therefore, the contour maps of the two-dimensional temperature mea-surement represent a cross section through the center of the atomized spray. For lack of space, only an abbreviated image series is shown here. The images were cropped to zoom in on details of the spray.

The contour maps represent the temporal development of the temperature distribution after initiation of the atomization process. The origin of the image length mat-ches the line of sight, Fig. 6, and resides 40 mm below the nozzle. At $t_{\mathrm{imag}} = 0.0$ s, the gas jets does not flow yet. Only the flow of molten metal can be observed. The gas jets interact with the melt and the disintegration begins 0.1 s later. The beginning of the spray forming is at $t_{\mathrm{imag}} = 0.3$ s. The spray cone is stabilized and the temperature distri-butions become approximately similar. During this spray condition, it can be seen that the breakup of the melt is situated near a length of −20 mm. Below that length the atomized melt shapes a hollow cone with an approximate length of 50 mm.

The development of a hollow cone is due to the cone-shaped form of the ceramic feeding tube. Even a small divergence of the liquid metal inflow from the vertical direction causes a rotation of the pre-filmed melt. Due to the conservation of angular momentum, the azimuthal velocity increases with decrease in the tube diameter. When the rotating melt leaves the nozzle, the centrifugal
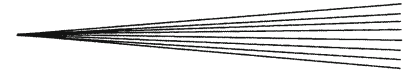
force acts perpendicular to the vertical axis. Thus, a rotating hollow cone is formed.

With further increase of the distance to the nozzle, the hollow cone disintegrates into ligaments and droplets. The iso-lines of the liquidus temperature show that up to a length between −60 and −80 mm the cooling down process from the temperature of the overheated melt to the liquidus temperature is completed.

These lengths are equivalent to distances of 100-120 mm from the nozzle to the lower end of the hollow cone. In terms of the diameter of the atomization nozzle, it means a distance to this nozzle of about 40 diameters. This averaged distance drawn from experimental data is in good qualitative agreement with the numerical results of the simulation by Gjesing et al. [14], where the models predict the beginning of the solidification process at a distance of 150 mm.

4. Conclusions

An optical two-color pyrometer for two-dimensional temperature measurements in metal atomization has been developed. The pyrometer is based on two standard industrial CCD-cameras with appropriate optical filters. Data analysis is performed using digital image processing. After calibration by means of a high-temperature furnace, the result is a relative measurement error smaller than 1.6% within the temperature range from 1273 to 1873 K.

The two-color pyrometer has been used during the process of metal atomization performed by means of a vacuum inert gas atomization facility. The measured average temperature distributions show the development of a hollow cone spray of the atomized metal. The average axial distance between the atomization nozzle and the region of the liquidus temperature was found approximately 40 times the diameter of the atomization nozzle.

Acknowledgments

References

1. B. Zheng and E.J. Lavernia, Melt Atomization, *Handbook of Atomization and Sprays: Theory and Applications*, N. Ashgriz, Ed., Springer, New York, 2011, p 837-848
2. J.R. Fincke, D.C. Haggard, and W.D. Swank, Particle Temperature Measurement in the Thermal Spray Process, *J. Therm. Spray Technol.*, 2001, **10**(2), p 255-266
3. P. Fauchais and M. Vardelle, Sensors in Spray Processes, *J. Therm. Spray Technol.*, 2010, **19**(4), p 668-694
4. B. Müller and U. Renz, Development of a Fast Fiber-Optic Two-Color Pyrometer for the Temperature Measurement of Surfaces with Varying Emissivities, *Rev. Sci. Instrum.*, 2001, **72**(8), p 3366-3374
5. G. Mauer, R. Vaßen, and D. Stöver, Plasma and Particle Temperature Measurements in Thermal Spray: Approaches and Applications, *J. Therm. Spray Technol.*, 2011, **20**(3), p 391-406
6. A. Vedaldi and B. Fulkerson, *VLFeat: An Open and Portable Library of Computer Vision Algorithms*, 2008, http://www.vlfeat.org/
7. G. Bradski and A. Kaehler, *Learning OpenCV: Computer Vision with the OpenCV Library*, O. Reilly Media, 2008, ISBN 978-0-596-51613-0
8. G. Mauer, R. Vaßen, and D. Stöver, Detection of Melting Temperatures and Sources of Errors Using Two-Color Pyrometry During In-flight Measurements of Atmospheric Plasma-Sprayed Particles, *Int. J. Thermophys.*, 2008, **29**, p 764-786
9. H. Chaves, S. Herbst, and C. Skupsch, Measurement of the Particle Velocity in a HVOF Spray with PIV Under Industrial Conditions, *J. Therm. Spray Technol.*, 2012, **21**(5), p 882-886
10. T. Dubberstein and H.-P. Heller, Effect of Surface Tension on Gas Atomization of a CrMnNi Steal Alloy, *Steel Res. Int.*, 2013, **84**(9), p 845-851
11. N. Zeoli, H. Tabbara, and S. Gu, CFD Modeling of Primary Breakup During Metal Powder Atomization, *Chem. Eng. Sci.*, 2011, **66**(24), p 6498-6504
12. G.S.E. Antipas, Review of Gas Atomization and Spray Forming Phenomenology, *Powder Metall.*, 2013, **56**(4), p 317-330
13. F. Träger, Ed., *Springer Handbook of Lasers and Optics*, Springer New York, 2007, ISBN 978-0-387-95579-7
14. R. Gjesing, J. Hattel, and U. Fritsching, Coupled Atomization and Spray Modeling in the Spray Forming Process Using Open-FOAM, *Eng. Appl. Comput. Fluid*, 2009, **3**(4), p 471-486